RSC Advances

PAPER

View Article Online
View Journal | View Issue

Cite this: *RSC Adv.*, 2020, **10**, 14262

High-efficiency adsorption and regeneration of methylene blue and aniline onto activated carbon from waste edible fungus residue and its possible mechanism

Hongyan Li, †*[a] Lianxin Liu,†[a] Jianguo Cui,[a] Jiali Cui,[a] Fang Wang[b] and Feng Zhang*[a]

Edible fungus residue as an efficient and low-cost precursor was used to produce Edible Fungus residue Activated Carbon (EFAC) using the zinc chloride activation method at a 1 : 2 impregnation ratio and 600 °C activation for 3 hours. The activation process does not need gases like nitrogen and is suitable for mass production. Fungal biodegradation facilitates efficient chemical activation, which might have generated abundant pores on the activated carbon sample. Using BET, X-ray diffraction (XRD), scanning electron microscopy (SEM), and FTIR characterization, reveals that EFAC exhibits a large specific surface area (1070 m^2 g^{-1}), and large pore volume (0.68 cm^3 g^{-1}), with its surface displaying a honeycomb-like structure. The EFAC adsorbs methylene blue (MB) and aniline in water, with maximum adsorptions of 662.25 and 27.10 mg g^{-1}, respectively. Various adsorption conditions, such as the EFAC dosage, pH, contact time and initial concentration were investigated. The adsorption is characterized by the pseudo-second-order kinetic and Langmuir isotherm models, with thermodynamics studies indicating that the adsorption is endothermic and spontaneous. Furthermore, the EFAC exhibited good regeneration performance by a 90% ethanol solution. The EFAC is a low-cost and environmentally friendly adsorbent for removing organic contaminants in wastewater.

Received 9th February 2020
Accepted 18th March 2020

DOI: 10.1039/d0ra01245a

rsc.li/rsc-advances

Introduction

Methylene blue (MB) and aniline are widely used in dyeing, printing, electroplating, tanning and related industries.[1,2] Around 10% of dyes containing MB and aniline used in industry are discharged into the environment, causing serious harm to the environment.[3] These pollutants cause allergies, skin irritation, and are even carcinogenic.[4] These pollutants that are difficult to biodegrade, when present in wastewater, have previously created ecological and environmental problems necessitating remediation.[5] At present, the main methods for treating MB and aniline wastewater are photocatalytic degradation,[6,7] membrane filtration,[8,9] advanced oxidation,[10,11] electrochemical methods[12,13] and adsorption.[14,15] Among these methods, adsorption is effective, economical, and exploitable.[16] Therefore, due to these advantages, adsorption is considered an effective method for treating dyes and aniline-containing wastewater.

The adsorption method depends significantly on the adsorption material, with existing materials affected by problems like high cost and low adsorption capacity.[6] Therefore, finding economic materials with high adsorption performance is crucial for treating dyes, and aniline-containing wastewater. Important water treatment technology involving activated carbon, indicates its adsorption developed pore structure, improved specific surface area, and exhibited a strong adsorption capacity.[17] These characteristics promoted the use of activated carbon in environmental governance including the chemical, pharmaceutical, food, printing, and dyeing industries. However, traditional activated carbon raw materials are expensive, causing the use of renewable agricultural waste to prepare activated carbon to gain significant attention, for example, fox nutshell,[4] walnut shell,[18] rattan of *Laccosperma secundiflorum*,[14] peanut husk,[19] corn cob,[20] apricot kernel,[21] pistachio hull,[22] and wodyetia bifurcate.[23] There are two main methods for making activated carbon: physical activation and chemical activation. Compared with physical activation, chemical activation requires lower temperature and shorter time. Activated carbon obtained by chemical activation has a larger specific surface area and rich micropores.[24] In addition, a large number of studies have used $ZnCl_2$ as activating agent of the carbon precursor.[25–27] Zinc chloride activation method gives

[a]*College of Environmental Science and Engineering, Taiyuan University of Technology, Jinzhong, Shanxi, 030600, China. E-mail: lihongyan002@tuyt.edu.cn*

[b]*Research Center for Edible Fungi, Biological Institute of Shanxi Province, Taiyuan, Shanxi, 030006, China*

† These authors contributed equally to this work and should be considered co-first authors.

activated carbon extremely high specific surface area and pore volume.

China, as a major agricultural producer, generates considerable amounts of agricultural residues annually. Among these, the edible fungus residue, a byproduct of mushroom harvesting, exceeds 100 million tons in output.[28] However, most edible fungus residues are discarded or burned, causing environmental pollution, discouraging cultivation of edible fungi, and hindering stable development of the edible fungus industry chain.[29] Edible fungus residue contains mainly sawdust and cottonseed hull, on which fungi grow. After the fungi decompose, the tissue structure is highly brittle, forming a loose precursor with a honeycomb-like structure. This structure facilitates penetration of the activator, ensuring an efficient chemical activation process, which might have generated abundant pores on the EFAC.[30] Therefore, edible fungus residue represents an economical and efficient raw material for the preparation of activated carbon. However, most of the research has focused on the use of edible fungus residue to improve the soil, as a substrate for plant cultivation, and it has not fully utilized its characteristics suitable as an activated carbon precursor.[31,32] Previous studies rarely examined the use of edible fungus residue for activated carbon preparation. In fact, no study reports adsorption of MB and aniline by activated carbon prepared from edible fungus residue.

The aim of this work is to use edible fungus residue as precursor material for preparing a low-cost, high pore volume, and good regeneration ability activated carbon involving the $ZnCl_2$ activation method. The preparation method is simple, practicable, and suitable for mass production. We studied the adsorption of MB and aniline in aqueous solution by the EFAC and discussed the mechanism, determined the optimal adsorption conditions for the EFAC to remove MB and aniline and its efficiency, discussed the kinetic, isotherm, and thermodynamic parameters, and conducted regeneration studies using chemical agents.

Materials and methods

Materials

The edible fungus residues are from Jinzhong, Shanxi, China. The raw materials were peeled, washed with distilled water, dried in an oven at 60 °C for 12 h, and crushed using an electrical grinder to obtain 30–60 mesh material. The HCl, NaOH, $ZnCl_2$, and H_2SO_4 were purchased from Beijing Chemical Plan Factory (China), while methylene blue and aniline were acquired from Tianjin Beichen Founder Reagent Factory (China). All chemicals were of analytical grade.

Preparation of adsorbent

The edible fungus residue (10 g) was mixed with a 50 mL solution of 10 g $ZnCl_2$, and the mixture was stored for 36 h. The impregnated material was activated in a muffle furnace at 600° for 3 h. After cooling naturally, the material was soaked in HCl (30% wt) to remove residual zinc, then washed with distilled water until pH was neutral. Finally, the sample was dried in an oven at 120 °C for 12 h and further dried at 80 °C for 12 hours. The prepared Edible Fungus residue Activated Carbon (EFAC) was crushed, passed through a 100-mesh sieve, and stored in an airtight container.

Characterization of EFAC

The surface functional groups of the samples were determined by FT-IR (Thermo IS5) at the wavelength interval 400–4000 cm^{-1}. The morphology each sample was characterized by a ZEISS GeminiSEM 300 scanning electron microscope (SEM). X-ray diffraction (XRD) was performed using a Bruker D8 Advance X-ray diffractometer under 5° min^{-1}. The BET specific surface areas were analyzed by an ASAP 2020 V4.02 (Mike Co., USA).

Batch adsorption study

Batch adsorption experiments were conducted in 100 mL for MB (100 mg L^{-1}) and aniline (10 mg L^{-1}) solutions in 150 mL Erlenmeyer flasks, with 0.04 g for MB, and 0.5 g for aniline added, and placed in a constant temperature vibrator at 25 °C and 180 rpm for 3 h. The concentrations were measured using a UV-visible spectrophotometer (Shanghai Jinghua Technology Instrument Co., Ltd., China). The absorbance measurements occurred at a wavelength of 665 nm for MB and 545 nm for aniline. The removal rate and adsorption capacity were calculated according to eqn (1) and (2) as:

$$\eta\% = \frac{C_0 - C_t}{C_0} \times 100\% \quad (1)$$

$$q_t = \frac{V(C_0 - C_t)}{W} \quad (2)$$

where C_0 (mg L^{-1}) is the initial concentration of the adsorbate; C_t (mg L^{-1}) is the real-time concentration of the adsorbate; q_t (mg g^{-1}) is the adsorption capacity of EFAC at time t; V (L) is the volume of the adsorbate solution used and W (g) is the weight of the adsorbent used.

Regeneration studies

All the regeneration studies were performed in 150 mL Erlenmeyer flasks. The EFAC samples with adsorbed MB and aniline were filtered, washed, dried, and regenerated using 1 mol L^{-1} of HCl, 90% ethanol, and 1 mol L^{-1} NaOH, sequentially and shaken at 25 °C for 4 h for regeneration. Then, the regenerated EFAC was again placed in the flask for adsorption, with the adsorption–regeneration process occurring in three cycles. These provided data for calculating the MB and aniline removal rate.

Results and discussion

Characterization of the EFAC

The N_2 adsorption–desorption isotherms of the EFAC are displayed in Fig. 1A, with the BET analysis results showing a significantly high specific surface area for the EFAC. The adsorption isotherm for the EFAC shows a high slope below

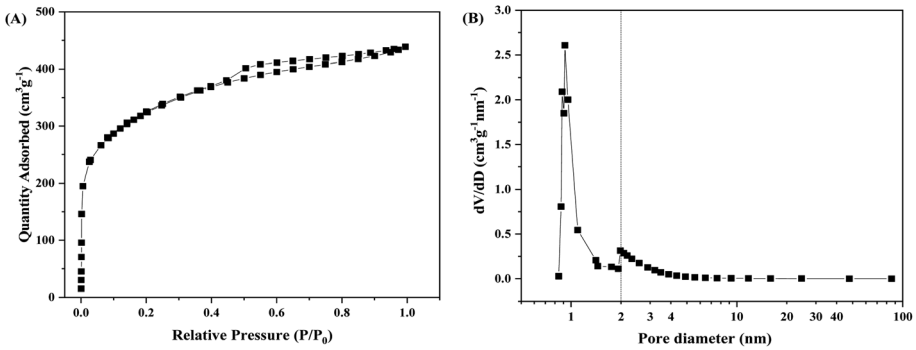

Fig. 1 (A) N_2 adsorption–desorption isotherm, (B) pore size distribution curve of EFAC.

relative pressure 0.1, and there is a type H4 hysteresis loop at relative pressure range 0.4–1.0, indicating that there are many micropores and slit-like mesopores.[33,34] The adsorption isotherms are type I and IV according to the IUPAC classification, suggesting that the material has both micropores and mesopores.[35] The BET surface area of EFAC is 1070 $m^2\ g^{-1}$, and the total pore volume is 0.68 $cm^3\ g^{-1}$, with an average pore diameter of 25.3 Å. The Barrett–Joyner–Halenda and Horvath–Kawazoe methods were used to calculate the pore size distribution and the results are displayed in Fig. 1B. The pores of the EFAC are mainly distributed around 0.9 nm and 2.0 nm, indicating the material is dominated by micropores and subordinate mesopores, which consistent with results from adsorption isotherms.

SEM images of the EFAC, MEFAC (EFAC with adsorbed MB), and AEFAC (EFAC with adsorbed aniline) are exhibited in Fig. 2A–E, respectively. Fig. 2A shows the EFAC magnification of 30 000 times. It can be seen that the surface of the prepared activated carbon is rough, has a porous structure, and has a small number of fine particles with a particle size ranging from 100 nm to 1 μm on the surface. Fig. 2B shows the image of EFAC magnified 15 000 times. The surface of EFAC presents a rough wrinkled structure with cracks and gaps arranged unevenly. Fig. 2C–E are EFAC, MEFAC, and AEFAC magnifications of 8000 times, respectively. The SEM analysis results reveal honeycomb-like porous structure of the surface of the EFAC, with pores ranging from one to tens microns. Among them, micropores are widely distributed, and the pore size distribution curve also proves this. Abundant microporous structure indicates great potential for pollutants to be adsorbed.[36] More pores facilitate the contact of organic molecules, thereby achieving efficient adsorption of dyes and aniline molecules. A large number of pores collapsed on the MEFAC are collapsed, while the surface is covered with fine particles. This indicates

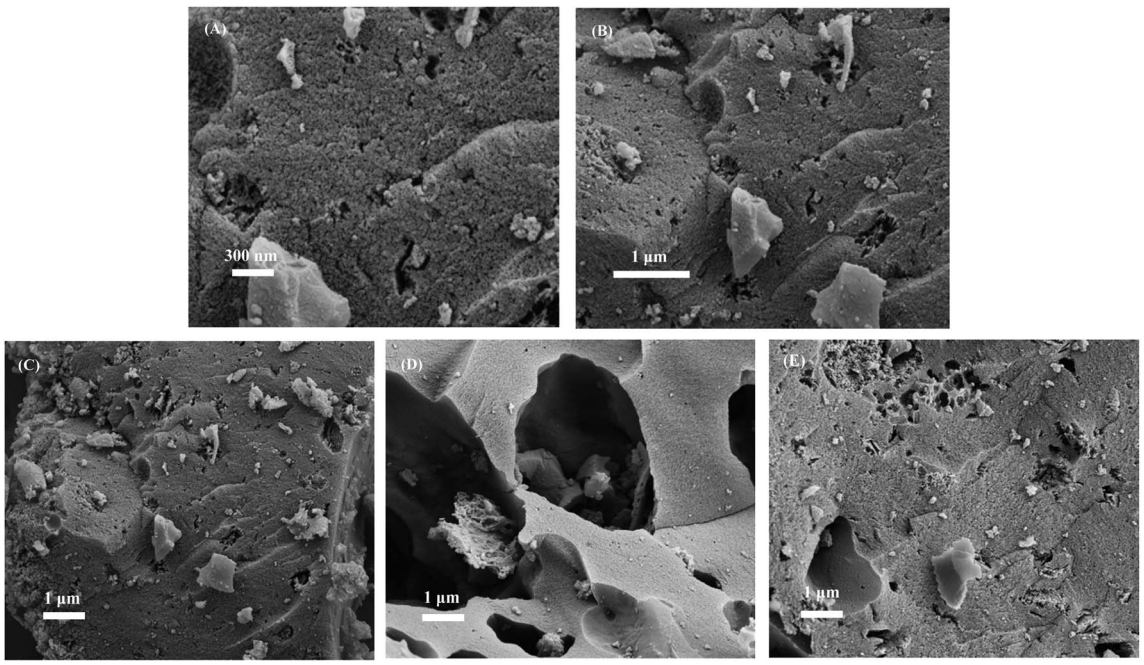

Fig. 2 SEM images of (A) EFAC magnification of 30 000 times, (B) EFAC magnification of 15 000 times, (C) EFAC magnification of 8000 times, (D) EFAC with adsorbed MB, and (E) EFAC with adsorbed aniline.

that the MB adsorption is more intense. The AEFAC surface also had some pores collapse, making the pore size distribution more uneven.

The FTIR spectrums of the EFAC before and after absorption are displayed in Fig. 3A to characterize the surface functional groups. The broad absorption peak around 3386 cm^{-1} is attributed to the O–H stretching vibration, while the weak and sharp absorption band around of 2920 cm^{-1} and 2840 cm^{-1} are the stretching vibration peak of the C–H bond of alkanes. The peak around of 2351 cm^{-1} corresponds to stretching vibration peak of the O–H bond in the –COOH functional group. The sharp peak at 1576 cm^{-1} reflects the C=O bond stretching vibration while the broad strong absorption peak around 1153 cm^{-1} is an anti-symmetric stretching vibration of the C–O–C bond on the surface of the material. After adsorption of MB, the peak around 3386 cm^{-1} caused by O–H stretching vibration was broadened and the peak intensity was enhanced, indicating that the hydroxyl groups on the EFAC surface and $-CH_2$ of MB formed hydrogen bonds, and MB were adsorbed to EFAC under the action of hydrogen bonding.[37] After aniline was adsorbed, the O–H peak became narrower and the peak intensity decreased, which may be caused by the consumption of hydroxyl groups during the adsorption process. The C=O peak at 1153 cm^{-1} became weaker in MEFAC but almost unchanged in AEFAC, this may be attributed to the higher affinity of the C=O functions towards MB compared with the aniline.[38] Only the intensity of the peak changed before and after the adsorption, indicating that the adsorption of MB and aniline by EFAC is a physical adsorption.

The crystal structure of EFAC was then analyzed by XRD, which is shown in Fig. 3B. Typical graphite structure characteristic absorption peaks appear at 2θ of 26.6° and 42.5° (JCPDS no. 26-1076). With peaks characteristic of graphite accumulation at 2θ of 26.6°, corresponding to the (004) diffraction surface, and the weaker diffraction peak at 2θ of 42.5°, corresponding to the (100) diffraction surface.

Effect of pH

We investigated relationship between the adsorption of MB and aniline by the EFAC and the solution pH. The pH of the solution was adjusted by using NaOH and HCl solutions at an initial concentration of 100 mg L^{-1} MB (0.04 g EFAC) and 10 mg L^{-1} aniline (0.5 g EFAC). Fig. 4A shows the effect of the EFAC adsorbing MB and aniline under different pH conditions (pH = 3.0–10.0), with pH clearly influencing the sorption. The pH point zero charge test was performed with reference to the methods reported in the previous literature.[39] Due to the EFAC contain active hydroxyl and carboxyl functional groups, it remove methylene blue and aniline mainly by electrostatic force and hydrogen bond. Under the different initial pH conditions, the pH of the solution increased slightly after EFAC adsorbed MB and aniline. When the MB adsorption reaction reached equilibrium, the pH values were 3.4, 5.5, 6.3, 7.4, 8.3, and 10.5. And for aniline the pH values at the time of 3.5, 5.3, 6.4, 7.5, 8.3, and 10.3. The increase in pH values during adsorption was due to the release of alkaline mineral ash on the surface of the EFAC.[33]

The MB is a cationic dye with an average molecular size of 1.43 × 0.61 × 0.4 nm, with its adsorption indicated to be influenced by solution pH previously.[40,41] Fig. 4A demonstrates that the removal rate of MB increases with pH rise (pH from 3 to 10). The experimental results show that the zero charge (pH_{pzc}) of EFAC is 6.93. When the pH < pH_{pzc}, the surface of the adsorbents have positively charged.[42] At pH below 5, the lower removal rate is attributed the positively charged surface of MB, creating competition of H^+ with the MB molecule. In addition, the electrostatic attraction of the MB and the surface of the EFAC is weak. As the pH increased, the anions on the activated carbon surface increased, with the anions neutralizing the positive charge on the surface, and eventually generating a negative charge on the surface of the adsorbent. The increased electrostatic attraction between the EFAC and MB then favors a higher removal rate.

Aniline is a weakly basic ionic compound, existing either as neutral or dissociated in aqueous solution.[43] The results in Fig. 4A display obvious removal of aniline under neutral conditions with a removal rate of 86.76% at a pH of 7. Under acidic and alkaline conditions, the removal efficiency decreased because the pH value likely affected the ionization morphology of aniline. Under acidic conditions, aniline mainly exists in the positively charged $C_6H_5NH^{3+}$ because of the high concentration of H^+. Meanwhile, the surface of the EFAC has positively

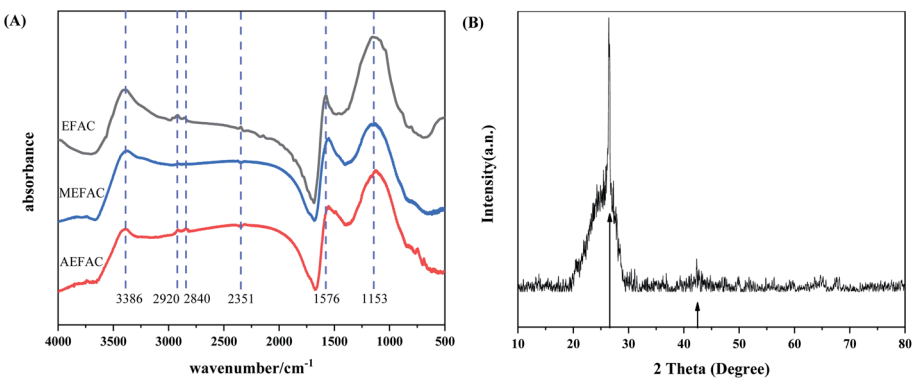

Fig. 3 (A) FTIR spectrum of EFAC before and after absorption, (B) XRD pattern of EFAC.

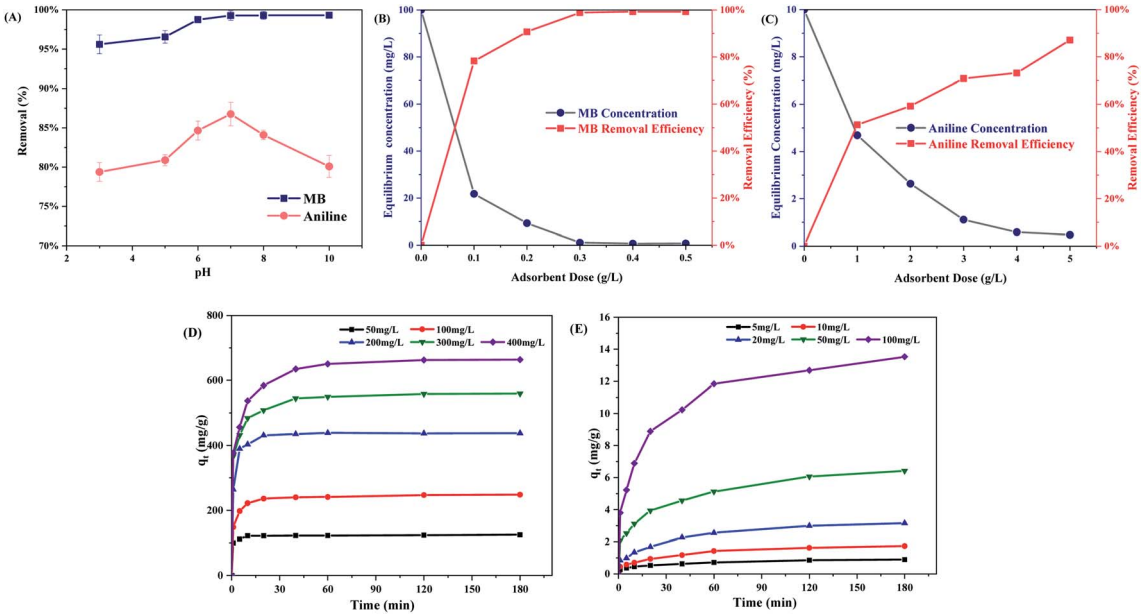

Fig. 4 (A) Effect of pH on the removal of MB and aniline by EFAC; (B) effect of the EFAC adsorbent amount on the removal and equilibrium concentration of MB; (C) effect of the EFAC adsorbent dose on the removal and equilibrium concentration of aniline; effects of contact time on the adsorption capacity at different initial concentrations of adsorbent mass: (D) 0.04 g for 100 mL MB solution and (E) 0.5 g for 100 mL anline solution.

charged when pH below pH_{pzc}. The $-COO^-$ on the surface of EFAC is low and the carboxyl groups mainly exist as –COOH. The electrostatic attraction of the EFAC and aniline is weakened, and the form of aniline at this time is not easily adsorbed by activated carbon. At higher pH value, the more negative charges on the surface of the activated carbon, and the stronger the adsorption capacity. In the alkaline environment, partially, many OH^- in the solution penetrate the EFAC cavities, competing with aniline for adsorption sites on the surface of the EFAC. Alternatively, aniline mainly exists in the molecular form $C_6H_5NH_2$, with low solubility. This is not conducive for the formation of hydrogen bonds, causing a lower removal rate.[44]

Effect of the adsorbent amount

The effect of adsorbent amount on MB and aniline removal was also studied using initial concentrations of 100 mg L^{-1} and 10 mg L^{-1} for MB and aniline, respectively. Fig. 4B shows the effect of the EFAC amount on the removal rate of MB, with the rate significantly increasing as the amount increased to 0.3 g L^{-1}. The increase in the adsorbed amount is attributed to the increase in the available adsorption sites. When the dosage is above 0.4 g L^{-1}, the removal rate remained basically unchanged. Therefore, to better remove pollutants and save materials, in subsequent experiments, we added 0.04 g of EFAC to the 100 mL solution. At equilibrium time, the removal rate reached 99.27% for an amount of 0.4 g L^{-1}. The adsorption of MB on the EFAC decreased from 782.16 mg g^{-1} to 198.46 mg g^{-1} with the amount of the adsorbent increasing from 0.1 to 0.5 g L^{-1}. For an amount of 0.1 g L^{-1}, the excess MB occupied the EFAC adsorption sites well and the contact rate between the adsorption site and MB decreased with increasing EFAC dosage.

Fig. 4C shows the effect of the EFAC amount on the aniline removal rate. The results indicate that the aniline removal rate increases rapidly with amount up to 5 g L^{-1}. More active sites were available for adsorption with increasing EFAC amount, thereby increasing the removal efficiency. The adsorption capacity per gram decreased as the EFAC amount increases due to the low driving force. The removal rate attained 87.10% for an amount of 5 g L^{-1} at equilibrium time. Therefore, in order to better remove methylene blue and reduce cost, we added 0.5 g EFAC to 100 mL aniline solution in subsequent experiments.

Effects of the contact time and initial MB and aniline concentrations

Fig. 4D and E reveal the effect of contact time on the adsorption of MB and aniline onto the EFAC under different initial concentrations. The adsorption capacity of the EFAC for MB and aniline significantly increases initially and then lowers, before stopping at equilibrium time. As the initial MB concentration increases, the adsorption equilibrium time also increased (Fig. 4D). The equilibrium time is 10 min at initial concentrations of 50 mg L^{-1}, 40 min at 100 mg L^{-1}, 60 min at 200 mg L^{-1}, and increased to 120 min at 300 mg L^{-1}. The initial concentration is an important driving force to overcome mass transfer resistance, and the adsorption capacity of the EFAC increases with the rising initial MB concentration. When the initial concentration of MB changes from 50 to 400 mg L^{-1}, the adsorption amount increased from 124.68 to 664.01 mg g^{-1}. The adsorption capacity of EFAC increases with the initial MB concentration because the initial concentration provided an important driving force to overcome the mass transfer resistance. More MB molecules are transported from the aqueous

solution to the EFAC surface, resulting in higher MB removal rate.[45]

The adsorption of aniline by EFAC is like that of MB. When the aniline initial concentration increased from 5 to 100 mg L^{-1}, the adsorption capacity increased from 0.89 to 12.63 mg g^{-1}, but the removal of 89.10% at 5 mg L^{-1} decreased to 63.16% at 100 mg L^{-1}. The adsorption capacity of EFAC increases with the initial aniline concentration because more aniline molecules are transported to the EFAC surface.

Adsorption kinetics of the EFAC

The study of kinetics is of great importance for understanding the adsorption dynamics and mechanism through the order of the rate constant.[46] The entire adsorption process can be fitted by kinetic models with the pseudo-first-order kinetic model, pseudo-second-order kinetic model, and intra-particle diffusion model commonly used. These three models were used to analyze the experimental data for removing MB and aniline in water by the EFAC.

The linear forms of the pseudo-first-order, pseudo-second-order kinetic models, and intra-particle diffusion model are expressed as:[33,47,48]

$$\ln(q_{e,cal} - q_t) = \ln q_{e,cal} - k_1 t \quad (3)$$

$$\frac{t}{q_t} = \frac{1}{k_2 q_{e,cal}^2} + \left(\frac{1}{q_{e,cal}}\right) t \quad (4)$$

$$q_t = k_i t^{0.5} + c \quad (5)$$

$$\chi = \frac{|q_{e,cal} - q_{e,exp}|}{q_{e,cal}} \quad (6)$$

where q_t (mg g^{-1}) is the adsorption amounts at time t, $q_{e,exp}$ (mg g^{-1}) and $q_{e,cal}$ (mg g^{-1}) are the equilibrium experimental results and calculated value according the model at the equilibrium

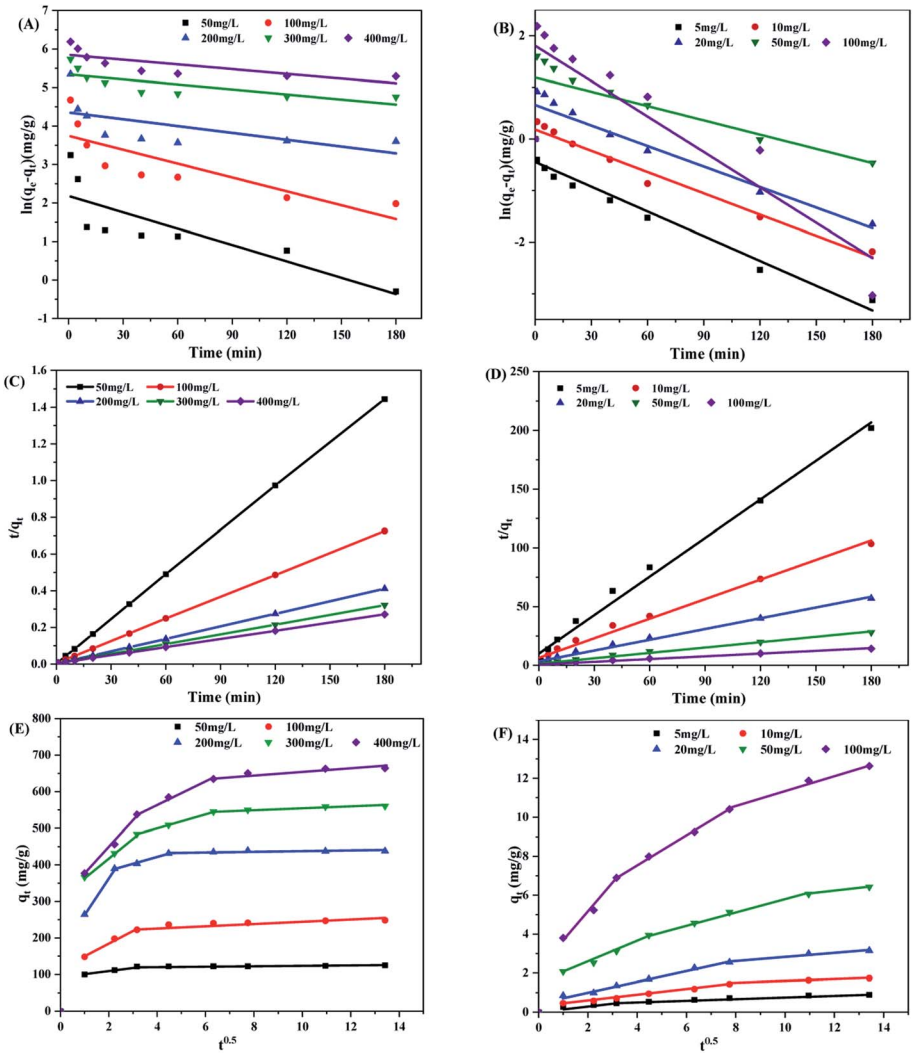

Fig. 5 (A) Pseudo-first-order model for the adsorption of MB onto the EFAC, (B) pseudo-first-order model for the adsorption of aniline onto the EFAC; (C) pseudo-second-order model for the adsorption of MB onto the EFAC; (D) pseudo-second-order model for the adsorption of aniline onto the EFAC; the intra-particle diffusion model for the adsorption of (E) MB and (F) aniline onto the EFAC.

time, respectively; k_1 (min^{-1}) is the quasi-first-order adsorption rate constant; k_2 (g min^{-1} mg^{-1}) is the quasi-second-order adsorption rate constant; k_i is the internal diffusion rate constant, t is the adsorption time, the intercept c reflects the boundary layer effect, and the χ is the relative error.

Kinetic experiments of pseudo-first-order and pseudo-second-order on the removal of w and aniline by the EFAC at five different concentrations are shown in Fig. 5A–D. The kinetic relative parameters of pseudo-first-order and pseudo-second-order are given in Table 1. The pseudo-first-order kinetics used to fit the R^2 values are lower, the calculated $q_{e,cal}$ are significantly different from the experimental values, and the χ are large. The pseudo-second-order kinetics, therefore, is more suitable for describing the adsorption of MB and aniline by the EFAC. The $q_{e,cal}$ calculated by this model match well with the experimental measurements. The adsorption process and adsorption capacity are faster for MB than aniline.

To further explore the adsorption process, the intra-particle diffusion model is used to fit the adsorption process of MB and aniline by the EFAC. Fig. 5E shows that the adsorption of high concentration MB (100–400 mg L^{-1}) by the EFAC comprises three straight lines, indicating that the adsorption process involves three stages: in the first stage, in the first few minutes of adsorption, the straight line slope is high and the intercept differs from zero, indicating that membrane diffusion is important in the rate control step. In the second stage, as the slope of the straight line decreases, the adsorption sites of the EFAC also decrease, highlighting the intra-particle diffusion process. In the third stage, the adsorption equilibrium stage was reached after 20 min of adsorption, with the adsorption sites were basically saturated. The adsorption process of the EFAC on MB (50 mg L^{-1}) was relatively fast, the adsorption process involves two stages and the adsorption equilibrium was attained within 10 minutes. Data in Fig. 5F the same trend for the adsorption process of MB and aniline. After aniline quickly occupied the adsorption sites on the EFAC surface, the remaining aniline are slowly transferred into the particles occupied the internal sites, and finally reach the adsorption equilibrium.

Adsorption isotherm of the EFAC

The adsorption isotherm reflects the surface adsorption characteristics in two phases when the adsorption equilibrium is reached at a certain temperature. Adsorption isotherms are important for analyzing adsorption mechanism. The Langmuir, Freundlich, Temkin, and Dubinin–Radushkevich (D–R) adsorption models are used to fit the data. Table 2 shows the relevant parameters of adsorption isotherm for MB and aniline on the EFAC.

The Langmuir adsorption model is suitable for single-layer homogeneous adsorption and it is described by eqn (6) expressed as follows:[49]

$$\frac{C_e}{q_e} = \frac{1}{R_L q_m} + \frac{C_e}{q_m} \quad (7)$$

where q_m (mg g^{-1}) is the maximum adsorption capacity of the adsorbent, R_L (L g^{-1}) is the empirical equilibrium constant, and C_e represents the affinity between the adsorbate and the adsorbent.

The Freundlich adsorption model is suitable for heterogeneous surface adsorption and expressed by eqn (7) as:[50]

$$\ln q_e = \ln k_F + \frac{1}{n} \ln C_e \quad (8)$$

where k_F and n are constants related to the adsorption capacity and adsorption strength, and $n > 1$ indicates that the adsorption performance of activated carbon is better.

The Temkin adsorption model represents a real state model, with the adsorption heat of the adsorbate decreasing linearly with increasing coverage, is expressed in eqn (8) as:[51]

$$q_e = B \ln(A) + B \ln C_e \quad (9)$$

where B is a constant related to heat of adsorption and A is the dimensionless isotherm constant.

The Dubinin–Radushkevich adsorption model considers that the size of the adsorbate molecule is close to the pore size of the microporous material, is expressed in eqn (9)–(11) as:[52]

Table 1 Kinetic constants obtained for the adsorption of MB and aniline onto EFAC at 25 °C

		C_0 (mg L^{-1})									
		MB					Anline				
Kinetic models	Parameters	50	100	200	300	400	5	10	20	50	100
Pseudo first-order	k_1 (min^{-1})	0.0142	0.0182	0.0059	0.0044	0.0041	0.0160	0.0137	0.0132	0.0092	0.0229
	$q_{e,cal}$ (mg g^{-1})	8.8651	38.335	77.953	209.03	346.63	0.6405	1.2006	1.9300	3.2869	6.0951
	R^2	0.6918	0.8096	0.3694	0.5792	0.5955	0.9600	0.9753	0.8951	0.5922	0.7372
	Δq_t	115.81	209.85	359.79	351.12	317.39	0.1904	0.4864	1.0633	3.6321	7.4371
	χ	13.064	5.474	4.6154	1.6798	0.9156	0.2973	0.4051	0.5509	0.1050	1.2202
Pseudo second-order	k_2 [g (mg min)$^{-1}$]	0.0169	0.0038	0.0043	0.0015	0.0009	0.1205	0.0488	0.0275	0.0167	0.0097
	$q_{e,cal}$ (mg g^{-1})	124.53	248.76	438.60	546.97	671.14	0.9142	1.7989	3.2714	6.5565	12.837
	R^2	0.9999	0.9999	1	0.9999	0.9999	0.9924	0.9913	0.9926	0.9926	0.9945
	Δq_t	0.15	0.60	0.86	13.18	7.12	0.0833	0.1119	0.2781	0.3625	0.6952
	χ	0.0012	0.0024	0.0020	0.0241	0.0106	0.0911	0.0622	0.0850	0.0553	0.0542

Table 2 Thermodynamic parameters for the adsorption of MB and aniline onto EFAC

		MB			Aniline		
Isotherms	Parameters	15	25	35	15	25	35
Langmuir	q_{max}	649.35	662.25	714.29	26.67	27.10	27.32
	R_L	0.1344	0.1795	0.1772	0.0242	0.0274	0.0296
	R^2	0.9846	0.9850	0.9869	0.9953	0.9933	0.9955
Freundlich	n	3.7509	4.5704	4.5704	2.1079	2.1872	2.2109
	K_F	9.3924	10.5066	10.5066	1.3038	1.3818	1.4147
	R^2	0.9599	0.9756	0.9856	0.9818	0.9791	0.9772
Tempkin	b	196.13	162.74	162.74	11.566	11.503	11.574
	A	2.5341	5.1582	5.1582	0.6368	0.6911	0.7145
	R^2	0.9767	0.9687	0.9687	0.9790	0.9721	0.9738
Dubinin–Radushkevich	q_{max}	477.71	480.97	464.38	19.58	16.20	16.54
	E	1581.1	3535.5	7453.6	100.00	353.55	408.25
	R^2	0.8455	0.8146	0.7037	0.8509	0.7043	0.7067

$$\ln q_e = \ln q_0 - \beta\varepsilon^2 \quad (10)$$

$$\varepsilon = RT \ln\left(1 + \frac{1}{C_e}\right) \quad (11)$$

$$E = \frac{1}{(2\beta)^{0.5}} \quad (12)$$

where β is the activity coefficient (mol^2 J^{-2}), E is the free energy of transfer for the adsorbate from the solution to the surface of adsorbent (kJ mol^{-1}), and ε is the Polanyi potential.

The fitting parameters in Table 2 reveal that the Tempkin adsorption isotherm equation cannot describe the adsorption process for MB and aniline well (R^2 = 0.9687, 0.9721). Compared with the fitting curves using the Freundlich model (R^2 = 0.9756, 0.9791), the Langmuir adsorption isotherm equation better represents the EFAC adsorption process of MB and aniline (R^2 = 0.9850, 0.9933). The results suggest that the adsorption occurs on the homogeneous surface of the EFAC, highlighting single-layer adsorption. Calculated from the Langmuir equation, the q_{max} of MB are 649.35, 662.25, and 714.29 mg g^{-1} at 15, 25, and 35 °C, respectively. Similarly, the q_{max} of aniline calculated from the Langmuir model are 26.67, 27.10, and 27.32 mg g^{-1} at 15, 25, and 35 °C, respectively. The R_L values are between 0–1 g L^{-1}, indicating that adsorption is favorable. The adsorption is an endothermic process. The increase of temperature increases the surface activity of the adsorbent, and the kinetic energy of the adsorbate increases, thereby improving the removal efficiency.[38]

The free energy was calculated by the D–R adsorption isotherm model, the energies of MB are 1.58, 3.54, and 7.45 kJ mol^{-1} at 15, 25, and 35 °C, respectively. And the energies of aniline are 0.10, 0.35, and 0.41 kJ mol^{-1} at 15, 25, and 35 °C, respectively. The energies of MB are significantly greater than that of aniline. The SEM images and regeneration effects also confirm this. The overall free energies are less than 8 kJ mol^{-1}, indicating that the adsorption process is mainly physical adsorption, intermolecular forces play an important role in the adsorption process.

From Table 3, the adsorption capacity calculated from Langmuir model of edible fungus residue activated carbon is higher than those of other adsorbents used to remove MB and aniline. According to these results, activated carbon prepared from edible fungus residue in this work is a promising material for removing hardly degradable organics contaminants in water.

Adsorption thermodynamics of the EFAC

During the adsorption process, thermodynamic parameters are important in controlling the adsorption behavior. The adsorption free energy (ΔG), the adsorption entropy (ΔS), and the adsorption enthalpy (ΔH) were calculated using eqn (12) and (13) expressed as follows:[59]

$$\Delta G = -RT \ln K \quad (13)$$

$$\ln K = \frac{\Delta S}{R} - \frac{\Delta H}{RT} \quad (14)$$

where ΔG (kJ mol^{-1}) is the standard Gibbs free energy change, ΔH (kJ mol^{-1}) is the standard enthalpy change, ΔS (J mol^{-1}) is the standard entropy change, K is the thermodynamic equilibrium constant, R (8.314 J (mol K)$^{-1}$) is the gas constant, and T (K) is the absolute temperature.

The experimental data at different temperatures were also analyzed and the related thermodynamic parameters for EFAC adsorption of MB and aniline are presented in Table 4.

According to various parameters, a positive ΔH indicates that the reaction is endothermic, with ΔH <40 kJ mol^{-1} indicating that the adsorption is mainly physical. The value of ΔG <0 suggests that the adsorption of the adsorbate from the solution to the carbon surface is a spontaneous process. This spontaneous process on the carbon surface verifies the feasibility of the adsorption of MB and aniline on the EFAC, with ΔS > 0 indicating that the EFAC is attractive for MB and aniline. During the adsorption process, the MB, and aniline molecules are replaced by water, thereby increasing entropy in the reaction system.

Table 3 Comparison of adsorption capacities of some sorbents and the EFAC

Adsorbents	Experimental conditions	q_{max} (mg g^{-1})	References
Methylene blue			
Phosphoric acid treated cotton stalk	$T = 35$ °C, pH = 7.0	222.22	53
Sludge-based activated carbon	$T = 30$ °C, pH = 7.0	158.73	5
Reed biochar	$T = 25$ °C, pH = 8.0	53.23	54
Wodyetia bifurcata biochar	$T = 25$ °C, pH = 7.0	149.34	23
Rattan activated carbon	$T = 30$ °C, pH = 7.0	359	14
BC-700	$T = 25$ °C, pH = 7.0	11.90	55
Edible fungus residue activated carbon	$T = 25$ °C, pH = 7.0	662.25	This work
Aniline			
Activated carbon/chitosan composite	$T = 20$ °C, pH = 7.0	22.9	56
Modified pine sawdust	$T = 20$ °C, pH = 6.2	21.8	57
Modied ATP	$T = 25$ °C, pH = 6.0	16.1	43
Cr-bentonite	$T = 30$ °C, pH = 4.4–5.0	21.6	58
RTAC	$T = 25$ °C, pH = 5.5	0.81	44
Edible fungus residue activated carbon	$T = 35$ °C, pH = 7.0	27.10	This work

Regeneration experiment

Adsorbent recovery is critical for reducing the cost of the adsorption process and recovering pollutants.[60] The analytical effects of three eluents: 1 mol L^{-1} HCl, 1 mol L^{-1} NaOH, and 90% ethanol were tested. Fig. 6 shows that the ethanol solution is the best desorbs MB and aniline from the EFAC. The removal rate of MB reaches 76.19%, 75.21%, and 62.53% of the original EFAC after 3 consecutive cycles by ethanol, sodium hydroxide, and hydrochloric acid, respectively. And the removal rate of aniline reaches 89.56%, 72.87%, and 87.81% of the original EFAC after 3 consecutive cycles by ethanol, sodium hydroxide, and hydrochloric acid, respectively. The experimental results show that 90% of ethanol regenerations are characterized by good recycling performances. After 3 regeneration cycles, the removal rate of 100 mg L^{-1} MB is still around 75.39% and 75.32% for the 10 mg L^{-1} aniline. Therefore, EFAC can be used as an efficient, economical and recyclable adsorbent for the treatment of wastewater containing MB and aniline.[61]

The adsorption capacity of EFAC after MB adsorption decreases rapidly during the regenerations, and after aniline adsorption, the adsorption capacity is basically unchanged. This is due to during the adsorption of MB, a large number of chemical reactions occurred on the surface of the EFAC, and the pore structure collapsed, so the adsorption capacity decreased greatly after regeneration, while the surface had less chemical interactions when adsorbing aniline, and the EFAC surface still maintained a good pore structure. After adsorption, the adsorption capacity is basically unchanged.

Adsorption mechanism

Based on the FTIR spectrums, BET, SEM characterization and adsorption experimental results, the mechanism of EFAC adsorption of methylene blue and aniline was analyzed. The intensity of the absorption peak changed after the adsorption, but no new characteristic absorption peak appeared, indicating that these functional groups contributed to the removal process, but no chemical change occurred. The adsorption of MB and aniline by the EFAC is mainly through physical adsorption. After adsorption of MB, the peak around 3386 cm^{-1} caused by O–H stretching vibration was significantly broadened and the peak intensity was also enhanced, indicating that MB was adsorbed to EFAC under the action of hydrogen bonding. After aniline was adsorbed, the O–H peak became narrower and the peak intensity decreased, which may be caused by the consumption of hydroxyl groups during the adsorption process. In addition, according to the effect of pH, it was found that electrostatic interaction has a great effect on the adsorption of MB and aniline. It is due to the EFAC has a large specific surface area, it can provide sufficient adsorption sites and has a large electronegativity. Fig. 7 shows that MB and aniline are adsorbed on the EFAC surface by electrostatic interaction, hydrogen bond, π–π interactions, and van der Waals forces.

The adsorption of MB by the EFAC mainly depends on the following:

As the pH increases, the removal rate increases, which indicates that electrostatic interaction between positively charged MB molecules and negatively charged surface functional groups on the EFAC promotes adsorption of MB molecules onto the surface of the EFAC. The existence of hydrogen bond between hydroxyl of the EFAC and nitrogen of MB could also be attributed to the MB adsorption.[62] Oxygen-containing groups on the EFAC surface like –COOH and –COH can

Table 4 Thermodynamic parameters for the adsorption of MB and aniline on the EFAC

Adsorbents	T (K)	ΔG (kJ mol^{-1})	ΔH (kJ mol^{-1})	ΔS (J mol^{-1} K^{-1})
MB	288.15	−11.85	10.33	76.97
	298.15	−12.62		
	303.15	−13.39		
Anline	288.15	−7.65	7.45	52.40
	298.15	−8.17		
	303.15	−8.70		

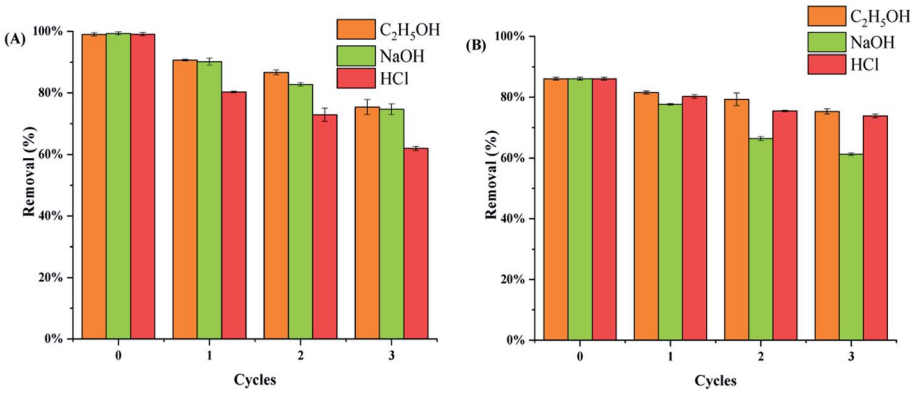

Fig. 6 Effect of regeneration times on (A) MB and (B) aniline adsorption by the EFAC.

adsorb some MB molecules through hydrogen bonding. Since MB is a planar molecule with an aromatic ring, the p-electrons existing in the molecular structure of MB and the p-electrons on the surface of EFAC will couple to form π–π bonds, thereby promoting adsorption of the MB molecules on the surface. In addition, intermolecular van der Waals forces are also a reason for MB adsorption.

Three adsorption routes seem acceptable for the aniline adsorption studies:

First, all –OH on the surface of the EFAC can form hydrogen bonds (O–H···N bond) with the amide group of aniline, and the oxygen atom on the surface can form hydrogen bond with the $–NH_2$ of aniline. The van der Waals force and the π–π bond also account for the adsorption of aniline. The aniline aromatic ring (electron acceptor) and the carboxyl oxygen (electron donor) of the EFAC form a donor–acceptor complex. In addition, the competitive adsorption of solvent molecules affected the adsorption of aniline by the EFAC. When the active adsorption site is blocked by solvent molecule adsorption, the solvent molecules can block some pores, and the adsorption site cannot contact the aniline molecules.

From the results of characterization, adsorption kinetics and isothermal adsorption tests, it can be seen that EFAC adsorbs MB more effectively than aniline. In terms of molecular structure, aniline has a typical aromatic amine structure: the aromatic ring with an amine group. By contrast, methylene blue has two nitrogen atoms and two aromatic rings, and its molecular weight is larger than aniline, which makes the hydrogen bonds, π–π bonds, and intermolecular forces between methylene blue and activated carbon stronger. This greatly increases the adsorption of methylene blue by activated carbon. The above is the reason that maximum adsorption observed in case of methylene blue and very less for aniline.

Cost analysis

The use of agricultural waste edible fungus residues to prepare activated carbon solves the problem of edible fungus residues disposal in China, it also introduces "treating waste with waste" and convert low-cost edible fungus residues to high-value activated carbon for the removal of pollutants like MB and aniline in wastewaters. The EFAC exhibits strong economic and environmental benefits, with its simple preparation process. Its operation even under aerobic conditions, without need for gases like nitrogen, suggests it is suitable for mass production. The prepared EFAC shows a high specific surface area, and calculated removal rates indicate good treatment on the typical dye, MB, and the refractory organic aniline.

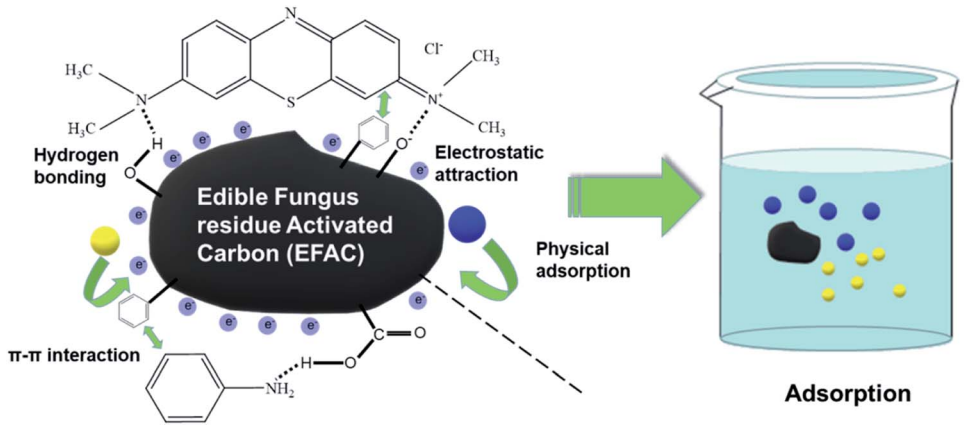

Fig. 7 Possible mechanisms for adsorption of MB and aniline on the EFAC.

Table 5 The estimated cost of 1 kg of EFAC from Fox nutshell ($ per kg)

Projects	Cost of making analytical-grade EFAC/($ per kg)	Cost of making commodity-level EFAC/($ per kg)
Raw materials	0.12	0.01
Zinc chloride	7.86	5.00
Hydrochloric acid + distilled water	0.45	0.40
Energy consumption	3.20	0.75
Total	11.63	6.16

According to calculations for data presented in Table 5, the cost of producing 1 kg of commercial EFAC is $6.16. This price is lower than that for commercially available activated carbon, with its excellent. Through experiments for comparison, commercially available activated carbon (North Fort industrial area in Dongli District, Tianjin Huaming Street, China) was found to adsorb 172.11 mg g^{-1} of the 100 mg L^{-1} MB compared to 248.18 for EFAC under the same conditions.

Conclusions

In this study, a low-cost and high-efficiency adsorbent, the EFAC, was produced from agricultural waste edible fungal residues, with N_2 not required during the production process. The prepared activated carbon showed a high specific surface area (1070 m^2 g^{-1}) and a honeycomb-like structure. The maximum quantity adsorbed was 662.25 mg g^{-1} for MB and 27.10 mg g^{-1} for aniline. The adsorption of MB and aniline followed the pseudo-second-order kinetic model and Langmuir adsorption model. The EFAC yielded 99.27% removal efficiency for MB and 86.74% for aniline in water. The material exhibited good regeneration performance by ethanol. Compared with ordinary commercial activated carbon, the EFAC is associated with lower cost, and higher adsorption efficiency. Therefore, the EFAC is a promising material for removing hardly degradable organic contaminants in water.

Conflicts of interest

There are no conflicts to declare.

Acknowledgements

The research was supported by Shanxi Province Graduate Education Innovation Project (Grant No. 2019SY132), Research and Development Plan Projects of Shanxi Province (Grant No. 201803D31046), and the Special Project for Transformation and Guidance of Scientific and Technological Achievements of Shanxi Province (Grant No. 201904D131065).

References

1 D.-W. Gao, Q. Hu, H. Pan, J. Jiang and P. Wang, *Bioresour. Technol.*, 2015, **193**, 507–512.
2 M. Ghaedi, A. M. Ghaedi, F. Abdi, M. Roosta, A. Vafaei and A. Asghari, *Ecotoxicol. Environ. Saf.*, 2013, **96**, 110–117.
3 A. Ahmad, S. H. Mohd-Setapar, C. S. Chuong, A. Khatoon, W. A. Wani, R. Kumar and M. Rafatullah, *RSC Adv.*, 2015, **5**, 30801–30818.
4 A. Kumar and H. M. Jena, *J. Clean. Prod.*, 2016, **137**, 1246–1259.
5 W.-H. Li, Q.-Y. Yue, B.-Y. Gao, Z.-H. Ma, Y.-J. Li and H.-X. Zhao, *Chem. Eng. J.*, 2011, **171**, 320–327.
6 F. Gulshan, S. Yanagida, Y. Kameshima, T. Isobe, A. Nakajima and K. Okada, *Water Res.*, 2010, **44**, 2876–2884.
7 W. Chu, W. K. Choy and T. Y. So, *J. Hazard. Mater.*, 2007, **141**, 86–91.
8 K. S. Lazarev, A. A. Arzamastsev, S. V. Kovalev and O. A. Abonosimov, *Condensed Matter and Interphases*, 2012, **14**, 203–207.
9 M. Soniya and G. Muthuraman, *J. Ind. Eng. Chem.*, 2015, **30**, 266–273.
10 T. Vescovi, H. M. Coleman and R. Amal, *J. Hazard. Mater.*, 2010, **182**, 75–79.
11 I. Y. Sapurina and J. Stejskal, *Russ. J. Gen. Chem.*, 2012, **82**, 256–275.
12 Y. H. Han, X. Quan, S. Chen, H. M. Zhao, C. Y. Cui and Y. Z. Zhao, *Sep. Purif. Technol.*, 2006, **50**, 365–372.
13 E. Bayram and E. Ayranci, *Environ. Sci. Technol.*, 2010, **44**, 6331–6336.
14 M. A. Islam, M. J. Ahmed, W. A. Khanday, M. Asif and B. H. Hameed, *Ecotoxicol. Environ. Saf.*, 2017, **138**, 279–285.
15 H. Al-Johani and M. A. Salam, *J. Colloid Interface Sci.*, 2011, **360**, 760–767.
16 X. Cui, H. Hao, C. Zhang, Z. He and X. Yang, *Sci. Total Environ.*, 2016, **539**, 566–575.
17 H. Wu, R. Chen, H. Du, J. Zhang, L. Shi, Y. Qin, L. Yue and J. Wang, *Adsorpt. Sci. Technol.*, 2019, **37**, 34–48.
18 X. Y. Gao, L. Wu, W. J. Wan, Q. Xu and Z. Y. Li, *Int. J. Chem. React. Eng.*, 2018, **16**, 10.
19 W. Cai, J. Wei, Z. Li, Y. Liu, J. Zhou and B. Han, *Colloids Surf., A*, 2019, **563**, 102–111.
20 H. Li, P. Gao, J. Cui, F. Zhang, F. Wang and J. Cheng, *Environ. Sci. Pollut. Res.*, 2018, **25**, 20743–20755.
21 F. Sabermahani, N. M. Mahani and M. Noraldiny, *Toxin Rev.*, 2017, **36**, 154–160.
22 H. Jalayeri and F. Pepe, *Ecotoxicol. Environ. Saf.*, 2019, **168**, 64–71.
23 K. J. Leite dos Santos, G. E. de Souza dos Santos, I. M. Gomes Leite de Sa, A. H. Ide, J. L. da Silva Duarte, S. H. Vieira de

Carvalho, J. I. Soletti and L. Meili, *Bioresour. Technol.*, 2019, **293**, 122093.
24 T. Budinova, E. Ekinci, F. Yardim, A. Grimm, E. Björnbom, V. Minkova and M. Goranova, *Fuel Process. Technol.*, 2006, **87**, 899–905.
25 H. Cherifi, B. Fatiha and H. Salah, *Appl. Surf. Sci.*, 2013, **282**, 52–59.
26 N. A. Khan, S. Shin and S. H. Jhung, *Chem. Eng. J.*, 2020, **381**, 7.
27 H. Ma, Z. Xu, W. Wang, X. Gao and H. Ma, *RSC Adv.*, 2019, **9**, 39282–39293.
28 J. K. Liu, S. Z. Wu, H. T. Cheng, G. Y. Li, Y. Li, J. C. Wang and Q. F. Li, *Chinese Journal of Tropical Crops*, 2019, **40**, 191–198.
29 R. R. Lew, *Nat. Rev. Microbiol.*, 2011, **9**, 509–518.
30 P. Wang, H. Ye, Y.-X. Yin, H. Chen, Y.-B. Bian, Z.-R. Wang, F.-F. Cao and Y.-G. Guo, *Adv. Mater.*, 2019, **31**, 1805134.
31 B. Li-li, Y. Tie-jun, W. Bin, B. Lin, T. De-gui, F. Xiang-chao and J. Agric, *Sci. Technol.*, 2013, **15**, 1069–1081.
32 J. M. Zhou, *Compost Sci. Util.*, 2017, **25**, 120–129.
33 A. A. Oladipo, E. O. Ahaka and M. Gazi, *Environ. Sci. Pollut. Res.*, 2019, **26**, 31887–31899.
34 A. A. Oladipo, A. O. Ifebajo and M. Gazi, *Appl. Catal., B*, 2019, **243**, 243–252.
35 K. S. W. Sing, *Pure Appl. Chem.*, 1985, **57**, 603.
36 M. A. A. Zaini, M. Zakaria, S. H. Mohd.-Setapar and M. A. Che-Yunus, *J. Environ. Chem. Eng.*, 2013, **1**, 1091–1098.
37 L. Jiang, L. Liu, S. Xiao and J. Chen, *Chem. Eng. J.*, 2016, **284**, 609–619.
38 A. A. Oladipo and A. O. Ifebajo, *J. Environ. Manage.*, 2018, **209**, 9–16.
39 L. D. T. Prola, E. Acayanka, E. C. Lima, C. S. Umpierres, J. C. P. Vaghetti, W. O. Santos, S. Laminsi and P. T. Djifon, *Ind. Crops Prod.*, 2013, **46**, 328–340.
40 Y. Gokce and Z. Aktas, *Appl. Surf. Sci.*, 2014, **313**, 352–359.
41 C. Pelekani and V. L. Snoeyink, *Carbon*, 2000, **38**, 1423–1436.
42 A. A. Oladipo, A. O. Ifebajo, N. Nisar and O. A. Ajayi, *Water Sci. Technol.*, 2017, **76**, 373–385.
43 Q. Deng, C. Chen, Q. Lei, J. Liang, T. Zhang and J. Jiang, *RSC Adv.*, 2018, **8**, 23382–23389.
44 V. K. Gupta, A. Nayak and S. Agarwal, *Chem. Eng. J.*, 2012, **203**, 447–457.
45 M. H. Marzbali, M. Esmaieli, H. Abolghasemi and M. H. Marzbali, *Process Saf. Environ. Prot.*, 2016, **102**, 700–709.
46 K. Li, M. Zhou, L. Liang, L. Jiang and W. Wang, *J. Colloid Interface Sci.*, 2019, **546**, 333–343.
47 R. Zhao, Y. Wang, X. Li, B. L. Sun and C. Wang, *ACS Appl. Mater. Interfaces*, 2015, **7**, 26649–26657.
48 L. H. Dong, W. J. Liu, R. F. Jiang and Z. S. Wang, *Bioresour. Technol.*, 2014, **171**, 260–264.
49 I. Langmuir, *J. Am. Chem. Soc.*, 2002, **40**, 1361–1403.
50 H. Freundlich, *Z. Phys. Chem., Stoechiom. Verwandtschaftsl.*, 1906, **57**, 385–470.
51 R. Kumar, R. K. Sharma and A. P. Singh, *J. Mol. Liq.*, 2017, **232**, 62–93.
52 M. M. Dubinin, *Carbon*, 1985, **23**, 373–380.
53 H. Deng, J. Lu, G. Li, G. Zhang and X. Wang, *Chem. Eng. J.*, 2011, **172**, 326–334.
54 Y. Wang, Y. Zhang, S. Li, W. Zhong and W. Wei, *J. Mol. Liq.*, 2018, **268**, 658–666.
55 Y. Dai, J. Li and D. Shan, *Chemosphere*, 2020, **238**, 124432.
56 R. Huang, B. Yang, Q. Liu and Y. Liu, *J. Appl. Polym. Sci.*, 2014, **131**, 39903.
57 Y. B. Zhou, X. C. Gu, R. Z. Zhang and J. Lu, *Ind. Eng. Chem. Res.*, 2014, **53**, 887–894.
58 H. Zheng, D. Liu, Y. Zheng, S. Liang and Z. Liu, *J. Hazard. Mater.*, 2009, **167**, 141–147.
59 K. Rathinam, S. P. Singh, Y. L. Li, R. Kasher, J. M. Tour and C. J. Arnusch, *Carbon*, 2017, **124**, 515–524.
60 M. B. Ahmed, J. L. Zhou, H. H. Ngo, W. S. Guo and M. F. Chen, *Bioresour. Technol.*, 2016, **214**, 836–851.
61 M. Gazi, A. A. Oladipo and K. A. Azalok, *Sep. Sci. Technol.*, 2018, **53**, 1124–1131.
62 Y. Zhu, B. Yi, Q. Yuan, Y. Wu, M. Wang and S. Yan, *RSC Adv.*, 2018, **8**, 19917–19929.